Ablation behavior of electrode materials during high power and high repetition rate laser structuring

A. Meyer*[a], Y. Sterzl[a], S. Xiao[b], U. Rädel[c], W. Pfleging[a]
[a]Karlsruhe Institute of Technology, IAM-AWP, Hermann-von-Helmholtz-Platz 1, 76344 Eggenstein-Leopoldshafen, Germany;
[b]EdgeWave GmbH, Carlo-Schmid-Straße 19, 52146 Würselen, Germany;
[c]TOPAG Lasertechnik GmbH, Nieder-Ramstädter Str. 247, 64285 Darmstadt, Germany

ABSTRACT

Laser structuring is introduced to homogenize the wetting of electrodes with liquid electrolyte, to avoid or significantly shorten the process time of warm ageing, and to reduce the lithium-ion diffusion overpotential that occurs during high-performance operation or when thick-film electrodes are applied. For the integration of the laser structuring process into the cell production line, the process speed must be adapted to the electrode coating speed. Various strategies, including increasing the repetition rate and laser power, beam shaping, where the Gaussian beam is formed into a rectangular intensity profile (1D top-hat), and multibeam processing by beam splitting, are pursued here. In the presented study, a laser system providing an average pulse duration of 600 fs, repetition rates in the MHz range, and a maximum power of 300 W, was applied. The ablation results are compared to those of a ps laser system that operates at lower repetition rates. The ablation depth and width as well as the appearance of the structures depending on the applied maximum energy density, repetition rate, and structuring speed, were evaluated, while the pulse overlap was kept constant. It was shown that the use of very high repetition rates leads to a decrease in ablation depth as well as a widening of the manufactured grooves, as the developing of material vapor plasma and ejected particles modify the absorption of subsequent laser pulses. A maximal scanning speed of 1.7 m/s could be achieved for the laser structuring applying a Gaussian beam.

Keywords: Ultrafast laser ablation, anode, lithium-ion battery, upscaling, laser structuring, ablation behavior

1. INTRODUCTION

The ongoing electrification of the transportation sector, be it cars (hybrid or fully electric ones), scooters or bikes, but also the increasing demand for electrified toys and gadgets, call for an increasing production capacity of low-cost, high-power and high-energy lithium-ion cells. New production technologies and cell compositions have to be established to fulfill the market's demands, one of which is the laser patterning of the electrodes, which was proven to increase the rate capability and facilitate the usage of high thickness electrodes, so that the volumetric energy density and high energy capability can be improved simultaneously, which was proven by several authors, e.g., Zheng et al. [1, 2], Zhu et al. [3], Smyrek et al. [4], Pfleging et al. [5], Habedank et al. [6], Dubey et al. [7], Park et al. [8]. Thorough investigations of the ablation behavior of graphite, silicon/graphite composite, or NMC electrodes have not been performed yet, but for a full comprehension of the processes it is necessary to take a closer look, which will be done for graphite electrodes in this study.

The ablation behavior of graphite for a limited process parameter regime was studied by Habedank et al.[9]. They produced holes of 25 µm diameter in graphite anodes with a thickness of 50 µm. The holes were arranged in grid pattern with a distance of 70 µm and were paired with NMC cathodes in coin cells. At a C-rate of C/10, they achieved a capacity of 3.86 mAh. Compared to coin cells with unstructured anodes, an increase in specific capacity of 20 % could be observed at C-rates between 2C and 5C. At C rates lower than 1C, unstructured and structured electrodes exhibited similar specific discharge capacities. The improved performance was attributed to a reduction of diffusion overpotential due to shortened lithium-ion diffusion paths, while the similar discharge capacities at low C rates indicate that no damage from thermal effects occurred due to laser patterning with ps pulses. Habedank et al.[9] used an ultrashort pulsed laser source with a pulse length of 400 fs and a wavelength of 1040 nm with varying repetition rates (10 to 10,000 Hz) and pulse energies (max. 40 µJ) to generate the holes in the graphite electrodes. They showed that the ablation depth as function of the fluence F seems to follow the logarithmic ablation model first published by Nolte et al.[10] in 1997.

* Alexandra.meyer@kit.edu; phone: +49 721 608-28161

At a constant repetition rate of 10 Hz, the calculated ablation threshold and optical penetration depth decreased as the number of pulses increased. An influence of the number of pulses was therefore shown, which was already known to be the case for metals. Additionally, it was found that when the repetition rate increased while the F_{max} and number of pulses remained constant, the ablation depth decreased. It can be concluded that at high repetition rates, the ablation produced by the subsequent pulse is influenced by the processes caused by the previous pulse. Habedank et al.[9] attributed this influence to shielding effects by the ablated graphite particles as well as heat accumulation.

Kouli et al.[11] used a laser source with a wavelength of 1064 nm, a pulse width of 8.6 ps and a M^2 of 1.23 to generate a hole pattern in two double-side coated graphite electrodes with different thicknesses (63 µm and 119 µm). The repetition rate was varied between 400 kHz and 10,000 kHz, the number of pulses between 1 and 25 and the average power of the laser beam between 10 W and 60 W. As in [9], the ablation depth decreased with increasing repetition rate and with decreasing pulse peak fluence. Furthermore, three ablation phases could be identified. Laser structuring at a structure depth smaller than the layer thickness is characterized by a high ablation rate and increasing structure depth. If the structure depth is already in the order of magnitude of the coating thickness, interaction with the current collector occurs in addition to the interaction of the laser beam with the coating. This results in a decreasing ablation rate and an increasing hole diameter. The third phase describes the damage to the current collector and structuring of the underlying coating. In addition, Kouli et al.[11] observed a bulge around the holes. It was concluded that thermal effects may occur during ablation at high repetition rates, although a final clarification of the mechanisms for the formation of the bulge is still pending.

In the present study, a closer look will be taken at the ablation behavior of thick graphite electrodes which are laser patterned with two different laser sources. In contrast to Habedank et al.[9] and Kouli et al.[11], the ablation behavior of the electrodes is investigated when a line pattern is introduced, as it has been shown in [12] that this patterning exhibits enhanced wetting of the electrode with liquid electrolyte compared to point structures due to the capillary effect. Direct comparison between the literature and the presented study is therefore aggravated, as the pulse-to-pulse distance is added as another influencing factor. For the roll-to-roll processing in a production line, high scanning velocities have to be realized, so the upscaling of the patterning process is put into focus as well and a parallelized manufacturing with the implementation of diffractive optical elements is investigated.

2. METHODOLOGY

Graphite electrodes were prepared via ball milling. The composition of the electrodes is summarized in Table 1. A water-based 2.5 wt.% sodium carboxymethyl cellulose (CMC, MTI Corporation, USA) solution was prepared with a vacuum mixer (MSK-SFM-7, MTI Corporation, USA) and subsequently stirred for 24 h with a magnetic stirrer. The graphite (SPGPT808, Targray Inc., Canada), conductive carbon black (CB, C-nergy Super C65, Imerys G&C, Switzerland), and CMC solution were then premixed with a centrifugal mixer (Speedmixer DAC 150 SP, Hauschild, Germany). The slurry was homogenized with a ball mill (PULVERISETTE 7 premium line, Fritsch, Germany). A styrene-butadiene rubber solution with a solid content of 50 % (SBR, MTI Corporation, USA) was added and slowly stirred into the mixture with the centrifugal mixer. The solid content of the anode slurry was 33.33 %. The slurry was tape casted on a copper current collector (9 µm thickness, EQ-bccf-9u-180, MTI Corporation, USA) and dried at room temperature. The doctor blade distance was 450 µm. After drying, the electrodes were calendered to reach a calculated porosity of 40 %. The thickness of the electrodes after calendaring was 114 µm.

Table 1: Composition of the electrodes.

Material	**Mass fraction /wt.%**
Graphite	85
C65	5
CMC	5
SBR	5

The electrodes were ablated with a high-power, high repetition rate laser source (FX600-2-GFH, EdgeWave GmbH, Germany) with a wavelength of 1030 nm, a pulse length of 600 fs and a maximal average power of 300 W. The raw beam radius w_a were 1396 µm and 1279 µm in x- and y-direction, respectively ($M^2_x = 1.11$; $M^2_y = 1.01$). The laser seeder pulses run at frequency of 48.77 MHz, by working with a pulse picker several seeder frequency dividers can be set, corresponding to ten different pulse repetition rates between 48.77 MHz and 4.88 MHz. For the investigation of the ablation behavior of

the electrodes, the ratio of the laser scan speed to the repetition rate was kept constant to achieve a constant pulse overlap and a constant pulse-to-pulse distance of 0.1 µm. Different average laser powers were used between 12 W and 120 W, while the pulse energy E_p was kept constant:

$$\frac{v}{f} \approx 0.1\ \mu\text{m} = \text{const.} \tag{1}$$

$$E_p = \frac{P_{avg}}{f} = \text{const.} \tag{2}$$

The influence of the repetition rate during ablation with pulses of the same pulse peak fluence can therefore be compared. The repetition rates, scan speed, and associated seeder frequency divider (SFD) are summarized in Table 2. Additionally, experiments with varying average laser power (up to 240 W) and laser scan speed were conducted.

Table 2: Seeder frequency divider (SFD), repetition rates and scan speed for each repetition rate.

SFD	Repetition rate /MHz	Scan speed v /mm s^{-1}
1	48.772 ≈ 48.8	5000
2	24.368 ≈ 24.4	2500
3	16.257 ≈ 16.3	1667
4	12.193 ≈ 12.2	1250
5	9.7544 ≈ 9.8	1000
6	8.129 ≈ 8.1	833
7	6.967 ≈ 7.0	714
8	6.097 ≈ 6.1	625
9	5.419 ≈ 5.4	556
10	4.877 ≈ 4.9	500

A scanner (IntelliSCAN III 30, SCANLAB GmbH, Germany) and a F-theta lens (S4LFT2430/328, Sill Optics GmbH & Co. KG, Germany) were used. Additionally, two different setups of beam expansion telescopes (BETs) and plano-concave and plano-convex cylindrical lenses were utilized, as well as a diffractive optical element (DOE) to shape the beam and a beam splitter. The complete assembly is realized in a laser material processing system (PS450-TO, Optec S.A, Belgium). The optical setup is shown in Figure 1.

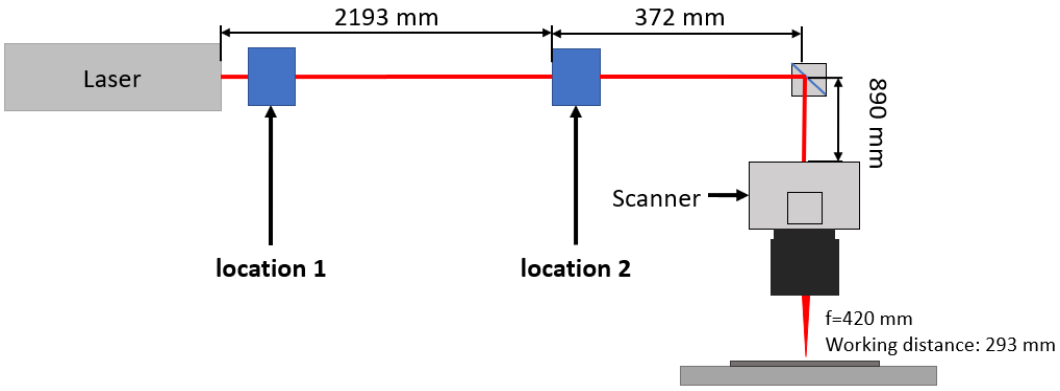

Figure 1: Optical setup with the laser beam source, the scanner and F-theta lens as well as two locations for different optical elements (BETs, DOEs).

At the location 1 and 2, different optical elements are included. For the “Setup 1”, a BET with an expansion of 2.2 is installed at location 1 and a BET with an expansion of 2.5 is installed at location 2. In the focus position, the beam therefore has a dimension of 39.14 µm in x-direction and 35.86 µm in y-direction. For the “Setup 2”, a beam shaper (FBS-L, TOPAG

Lasertechnik GmbH, Germany) is installed at location 1 and a cylindrical lens telescope with a plano-convex ((LJ1558RM-B, Thorlabs GmbH, Germany) and a plano-concave (LK1431RM-B, Thorlabs GmbH, Germany) lens are installed at location 2, as well as a beam splitter (DBS, TOPAG Lasertechnik GmbH, Germany). The beam splitter splits the beam in five equidistant beamlets.

The beam shaper is a diffractive optical element (DOE) which shapes the beam so that a one-dimensional top-hat is realized in the focus position. The length of the top-hat is three times as big as the diffraction-limited spot in the focus position and the width w_{TH} can be approximated with the focal length f, the beam diameter at laser exit w_{LE}, and the wavelength λ:

$$w_{TH} = \frac{\lambda \cdot f}{w_{LE}} \tag{3}$$

Depending on the position of the beam splitter compared to the cylindrical lens telescope (before / after), two different distances between the beamlets could be realized, namely about 1.01 mm and 0.25 mm. For the investigation of the ablation behavior with "Setup 2", a repetition rate of 4.9 MHz and a maximum power per beam of 34 W is applied.

During the evaluation of the fs laser source with "Setup 2", it became clear that higher powers are needed for a successful process parallelization, which was realized with a ps laser source (EdgeWave PX400-1-GF, EdgeWave GmbH, Germany). The laser source has an output beam diameter of 3 mm, a wavelength of 1064 nm and pulse length of 12 ps, with a maximum power of 400 W at the specified frequency (1 MHz). A 2 x beam expansion telescope, a scanner (IntelliScan 14 II, Scanlab, Germany) and a F-Theta lens with a focal length of 100 mm were installed in the beam path. The beam waist at the sample w_0 can be estimated with

$$w_0 \approx \frac{\lambda \cdot f}{\pi \cdot w_L} \cdot \sqrt{M^2} \tag{4}$$

where the beam radius w_L at the position of the last lens was 2.6 mm and M^2 was 1.2. The calculated beam waist w_0 was approximated to be 13.8 µm. Three repetition rates were applied (100 kHz, 500 kHz, 1 MHz), and with laser scanning speeds of 50 mm/s / 500 mm/s (100 kHz); 250 mm/s / 2500 mm/s (500 kHz) and 500 mm/s / 5000 mm/s (1 MHz) two different pulse-to pulse distances of 0.5 µm and 5 µm were assessed.

For the characterization of the ablation behavior, a digital microscope was used (VHX 5000, Keyence, Japan). The depth of the grooves was measured. With a scanning electron microscope (SEM, Phenom XL, Thermo Fisher Scientific Inc., USA) the structured surfaces were evaluated regarding crack formation, thermal-induced damage, and debris formation.

3. RESULTS AND DISCUSSION

3.1 Gaussian beam "Setup 1"

The ablation depth as function of the logarithm of the pulse peak fluence for selected repetition rates is shown in Figure 2. When the repetition rate is increased, the ablation depth for the same energy density declines. Between 0.20 and 0.43 J/cm², the slope of the curve increases. This behavior is also observed for the drilling of metals[10], where two ablation regimes are identified. For metals, the ablation depth d at lower fluences can be associated with the optical penetration depth δ_o, and at higher fluences with the effective heat penetration depth δ_h by

$$d = \delta_{o,h} \ln\left(\frac{F_a}{F_{th}^{o,h}}\right) \tag{5}$$

where F_a is the absorbed laser fluence and $F_{th}^{o,h}$ is the corresponding threshold ablation fluence.

Even though the ablation mechanisms of laser drilling and line structuring are not directly transferable between each other, since the fluence acting on the sample is not locally constant during line structuring due to the pulse offset and the Gaussian intensity distribution, it is still reasonable to assume that the ablation behavior during line structuring is also influenced by different penetration depth as a function of fluence, and that changes in ablation behavior can be observed, quite similar to the drilling process. It seems to be evident from Figure 2 that at constant laser fluence but with increasing repetition rate, the ablation depth is decreasing. For a fluence of 0.6 J/cm², the maximum ablation depth for a repetition rate of 4.9 MHz was 74.0 µm, for 16.3 MHz it was 58.9 µm, and for 48.8 MHz it was 46.4 µm.

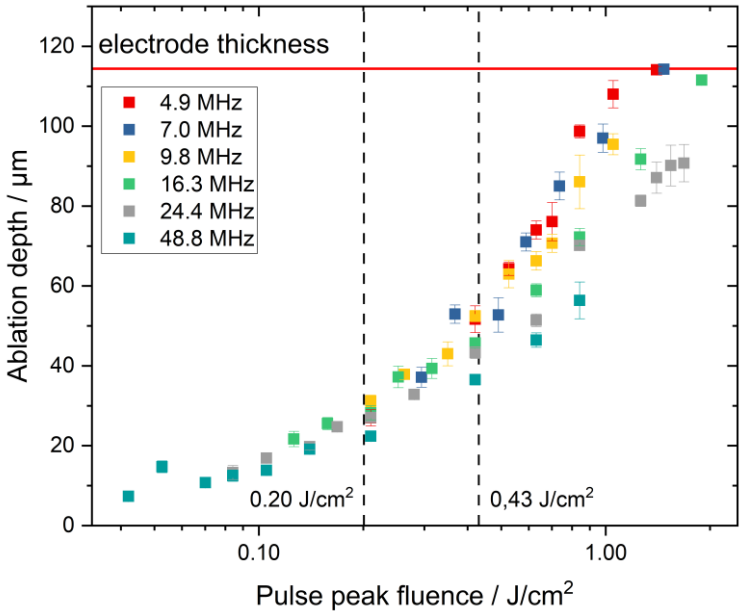

Figure 2: Ablation depth as function of pulse peak fluence for selected repetition rates.

In Figure 3, the ablation depth as a function of repetition rate for constant laser peak fluences of 0.21 J/cm² and 0.84 J/cm² is shown which confirms the described behavior. A decrease in ablation depth with increasing repetition rate is more pronounced when a higher fluence is applied. For the repetition rate of 4.9 MHz at 84 J/cm² an ablation depth of 98.7 µm was achieved, while at 48.8 MHz only 56.4 µm could be reached. This effect might result from the induced particle shielding and heat accumulation [13, 14].

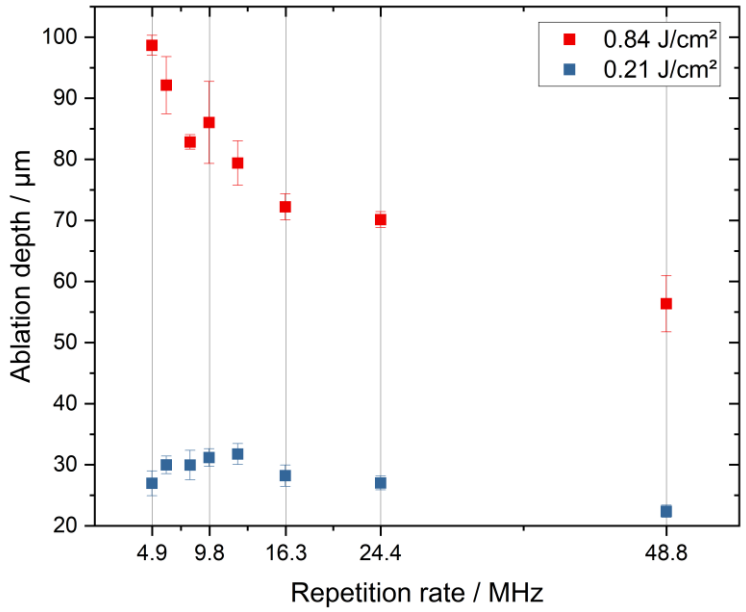

Figure 3: Ablation depth as a function of repetition rate for the energy density of 0.21 J/cm² and 0.84 J/cm².

For the upscaling of the electrode patterning process high laser scanning speeds need to be achieved. Figure 4 shows the ablation depth as function of the repetition rate for different average laser powers.

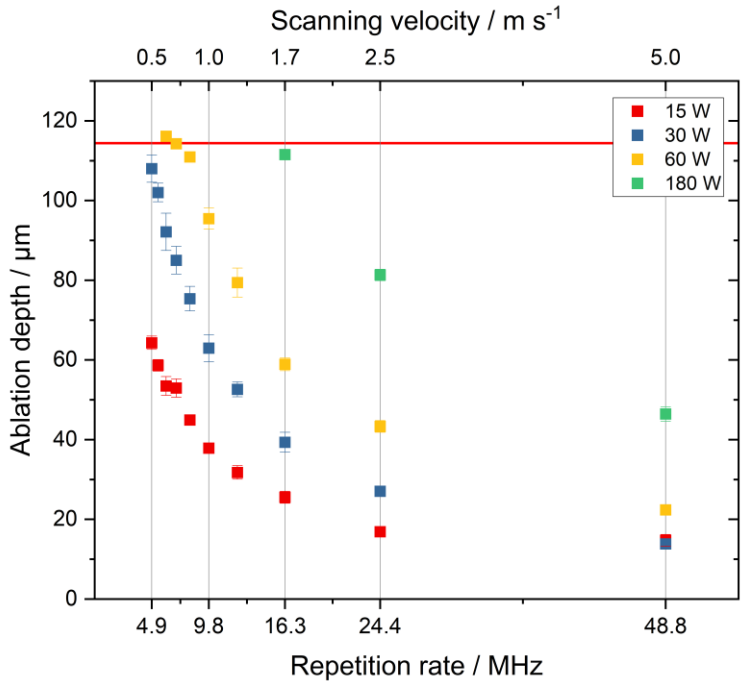

Figure 4: Ablation depth as function of the repetition rate or scanning velocity for different average laser powers.

Since the ratio between the scanning velocity and the repetition rate was kept constant, a dependence on the scanning velocity is also given. With increasing repetition rate or scanning velocity, the ablation depth which could be achieved at a certain average laser power is decreasing hyperbolically, while the ablation depth which could be achieved at a constant repetition rate increases with an increasing laser power. For an average laser power of 15 W, the current collector could not be exposed and the maximum ablation depth which could be reached for a scanning velocity of 0.5 m/s was 64.3 µm. When the average laser power is doubled (30 W), an ablation depth of 108.0 µm was achieved at a scanning speed of 0.5 m/s. When the power was doubled again (60 W), the current collector was damaged at 0.5 m/s, while at 0.7 m/s the electrode material was removed down to the current collector without damaging it, which therefore would be a usable parameter set. When the power is further increased (180 W), the current collector could be reached with a laser scan velocity of 1.7 m/s and a repetition rate of 16.7 MHz. This was the highest possible processing speed in frame of the presented study with the chosen parameter set.

3.2 Rectangular beam with beam splitting “Setup 2”

The intensity profile of the laser beam in focal plane after beam shaping DOE and cylindric lens telescope was measured with a CCD camera (WinCam-UCD12-UC, DataRay Inc., USA) and the profile is shown for a repetition rate of 4.88 MHz and an average laser power of 0.1 W in Figure 5 a) and b). The beam had a length of about 271 µm and a width of 65 µm. The intensity profile of the laser beam after the beam splitter was installed is shown in Figure 5 c). Five beamlets are clearly separated with a distance of 340 µm. The diffraction pattern showed equidistant second and higher-order maxima, which were deflected with an aperture before the scanner inlet, where a non-negligible amount of laser power was lost. The maximum power available at a repetition rate of 4.9 MHz was 170 W, compared to 260 W without beam splitter and DOE, which limited the power of each beamlet to 34 W. Due to pointing instabilities of the laser during changing the repetition rate, it would be necessary to adjust the optical elements for each repetition rate anew. This is not feasible and therefore only a repetition rate of 4.9 MHz was used.

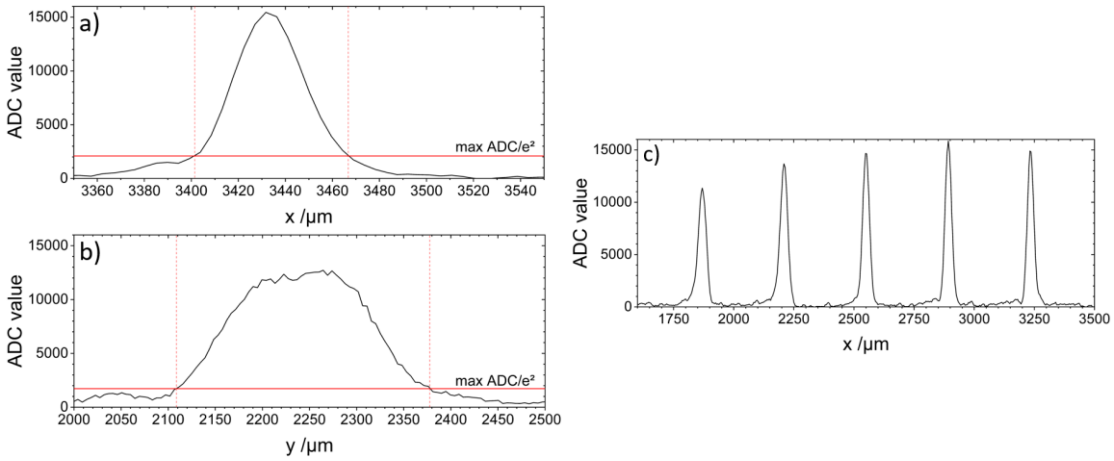

Figure 5: Shape of the beam in focal plane measured with a CCD camera a) with the beam shaper DOE in direction of beam shaping b) perpendicular to the beam shaping c) with the beam shaper and the beam splitter.

Due to the limitations in both repetition rate and power per beam, the experimental plan was adjusted, and for the mean power per beam of 20 W, 24 W and 30 W at a repetition rate of 4.9 MHz with a scanning velocity of 0.5 m/s the ablation depth as well as the width of the generated structures were investigated. These measurements can then be directly compared to Setup 1 with the same parameters, which is shown in Figure 6.

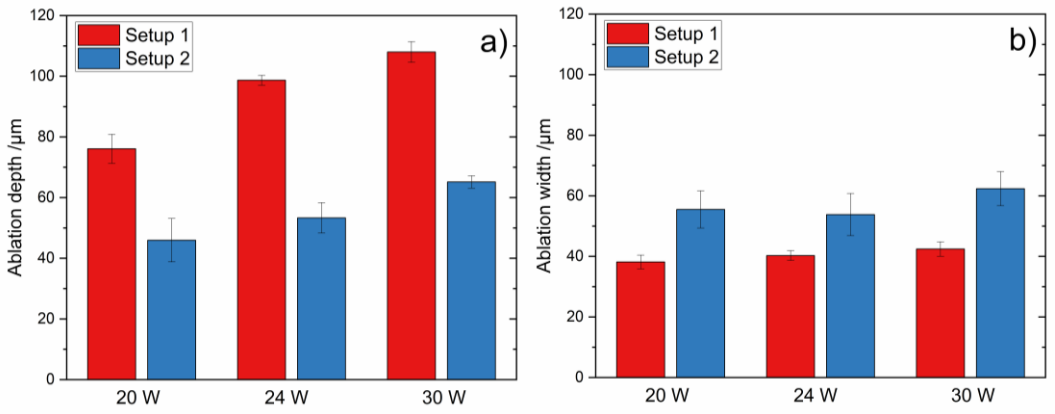

Figure 6: Comparison of a) ablation depths and b) ablation widths for laser powers of 20 W, 24 W and 30 W in Setup 1 and Setup 2.

The comparison between the ablation behavior of Setup 1 and Setup 2 shows a lower depth for the laser generated structures with Setup 2, while the width is increased. This can also directly be observed by scanning electron images, see Figure 7. Especially the width at the top of the electrode is increased immensely. The pulse overlap is also increased when the beam shaper is implemented, as the beam is about seven times longer compared to the Gaussian beam.

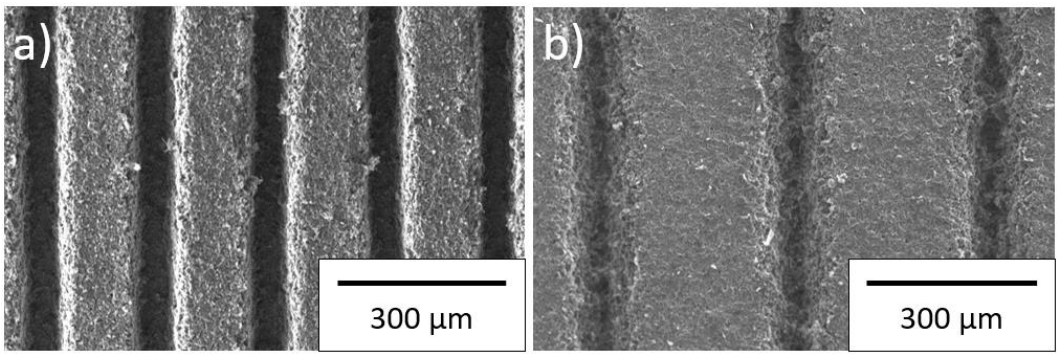

Figure 7: SEM images of the laser generated structures: a) Setup 1: 40 W laser power, 4.9 MHz repetition rate, 0.5 m/s scanning velocity; b) Setup 2: 30 W power (per beamlet), 4.9 MHz repetition rate, 0.5 m/s scanning velocity.

To compare the ablation behavior of the two setups with constant pulse overlap, additional experiments were conducted where the scan velocity in Setup 2 was increased to 3.5 m/s. The results are shown in Figure 8. When the pulse overlap is kept constant, a more significant assessment of the two different setups can be guaranteed. It was shown that Setup 2 shows an up to three times higher ablation depth for the same fluence, while the scanning velocity is increased sevenfold. With the implementation of the beam splitter and the resulting parallelization of the laser patterning process, the total scanning speed is increased by 35 times compared to Setup 1. But Figure 8 also shows that the energy density of the laser beam needs to be increased even further to realize a laser patterning where the electrode can be structured down to the current collector, since the maximum ablation depth which was reached was 80 µm.

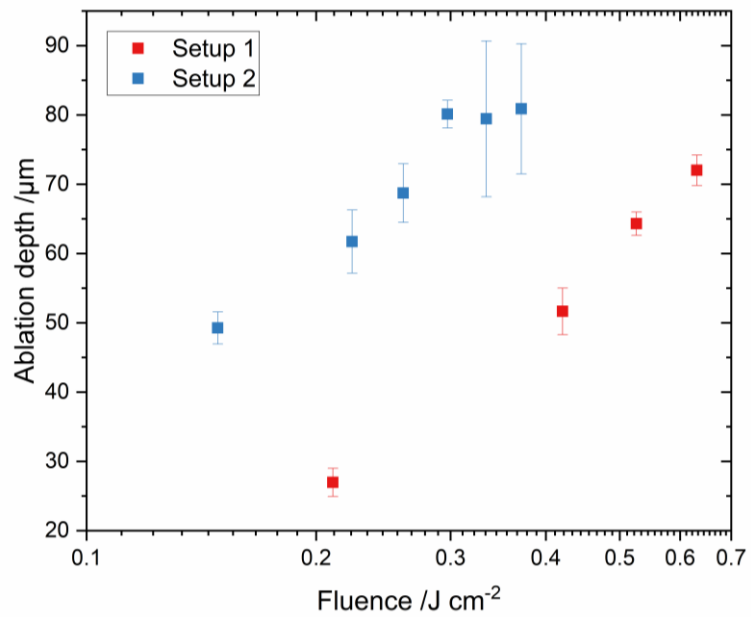

Figure 8: Comparison of ablation depth at a constant pulse-to-pulse distance of Setup 1 and Setup 2 for a repetition rate of 4.9 MHz and a scanning velocity of 0.5 m/s (Setup 1) and 3.5 m/s (Setup 2) as function of laser fluence.

3.3 Investigation of the ablation behavior with a ps laser source

When the power of the laser could be increased and the repetition rate could be decreased, higher fluences could be realized with “Setup 2”. The goal would be to increase the scanning speed by a factor of 7, as the laser beam profile is seven times longer in scanning direction. With an additional parallelization due to the implementation of a beam splitter the processing speed can be increased even more. For the laser patterning of electrodes for a standard 18650 cylindrical cell, a minimal belt speed of 35 m/min to 80 m/min, comparable to other electrode manufacturing steps[15], should be realized. Lower

repetition rates than 5 MHz and higher average laser powers than 260 W were realized with a ps laser source, which is able to deliver up to 400 W at 1 MHz. The ablation depth as function of the laser fluence is shown in Figure 9. With the smaller pulse-to-pulse distance of 0.5 µm the line structuring of the electrode reached the current collector at a fluence of approximately 13.4 J/cm² at a repetition rate of 500 kHz, and 16.7 J/cm² at a repetition rate of 1 MHz. The smaller pulse-to-pulse distance of 0.5 µm could not be realized with a repetition rate of 100 kHz, since the rather high energy densities lead to a destruction of the electrode and current collector. When the pulse-to-pulse distance of 5 µm was realized, i.e., the scanning velocity was increased by a factor of 10, the electrode could not be patterned until the current collector was reached, even when fluences over 100 J/cm² were applied. Here, even though the applied energy densities are two orders of magnitudes higher compared to the fluences in "Setup 1", since much lower repetition rates and a smaller beam waist were applied, a similar behavior as shown in Figure 2 could be observed showing two ablation regimes are present. The transition between the ablation regime dominated by the optical penetration depth and the effective heat penetration depth could be determined to lie between approximately 20 J/cm² and 50 J/cm².

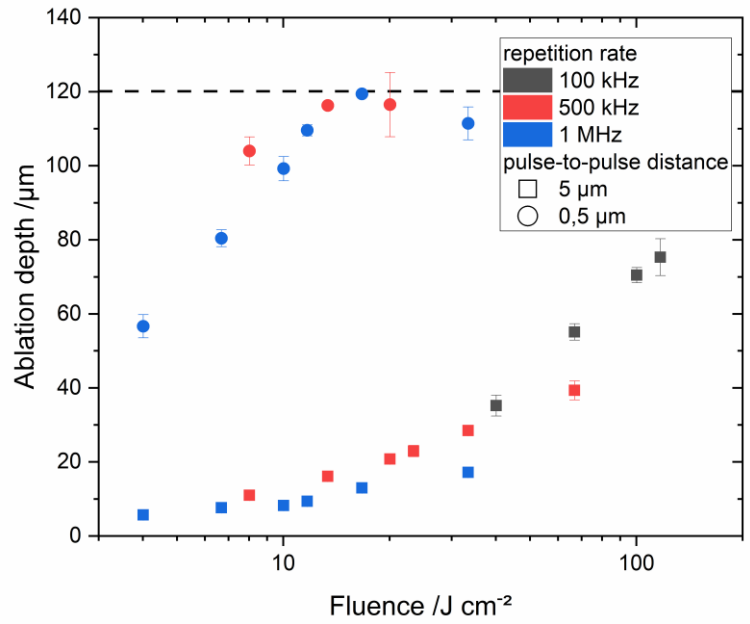

Figure 9: Ablation depth for the laser patterning process with a ps laser source for the repetition rates of 100 kHz, 500 kHz and 1 MHz for pulse-to-pulse distances of 5 µm and 0.5 µm.

4. CONCLUSION

The ablation behavior of graphite electrodes for the laser patterning process to accelerate the wetting process with liquid electrolyte and facilitate the application of very thick electrodes in lithium-ion cells due to the implementation of additional lithium-ion diffusion pathways was investigated depending on the applied energy density, repetition rate, and pulse-to-pulse distance. Two laser sources and three different optical setups were applied. For the establishment of a laser processing step of the electrodes in the lithium-ion cell manufacturing line, very high scanning speeds to keep up with the belt speed in a lithium-ion cell manufacturing line (approximately 35 m/min to 80 m/min [15]) need to be realized, and therefore a parallelization and acceleration of the process with the implementation of beam splitting and shaping optics was evaluated. When the ablation behavior of a thick graphite electrode is compared depending on the laser source, while both laser beams have a Gaussian shape, but different pulse widths (600 fs or 12 ps) and different repetition rates (min. 4.9 MHz or min. 100 kHz) are applied, similar observations could be noted. The ablation depth as function of the pulse peak fluence shows two ablation regimes, dominated by either the optical or the effective heat penetration depth. With increasing repetition rate, the ablation depth decreases, since there is an impact on the coupling of the subsequent laser pulse from the plasma and ejected material due to the preceding pulse.

It was proven that the implementation of laser beam shaping and beam splitting optical devices can increase the ablation depth at a constant laser fluence, while the scanning speed can be increased by a factor of seven. The comparison between

the ablation with and without beam shaper shows that similar ablation depths were achieved at 35 % to 45 % of the peak fluence compared to a Gaussian fluence profile at the same repetition rate (4,88 MHz) and pulse overlap.
Due to the dimensions of the shaped beam, rather high energy densities are required to ablate the electrode until the current collector is exposed. For future investigations, the implementation of a beam shaper DOE will be omitted, which facilitates higher energy densities due to smaller illuminated surfaces.

5. REFERENCES

[1] Zheng, Y., Seifert, H. J., Shi, H., Zhang, Y., Kübel, C. and Pfleging, W., "3D silicon/graphite composite electrodes for high-energy lithium-ion batteries," Electrochimica Acta 317, 502–508 (2019).

[2] Zheng, Y., Smyrek, P., Rakebrandt, J.-H., Kübel, C., Seifert, H. J. and Pfleging, W., "Fabrication and characterization of silicon-based 3D electrodes for high-energy lithium-ion batteries," SPIE Proceedings, 100920L (2017).

[3] Zhu, P., Seifert, H. J. and Pfleging, W., "The Ultrafast Laser Ablation of Li(Ni0.6Mn0.2Co0.2)O2 Electrodes with High Mass Loading," Applied Sciences 9(19), 4067 (2019).

[4] Smyrek, P., Zheng, Y., Rakebrandt, J.-H., Seifert, H. J. and Pfleging, W., "Investigation of micro-structured Li(Ni 1/3 Mn 1/3 Co 1/3)O 2 cathodes by laser-induced breakdown spectroscopy," SPIE Proceedings, 100920S (2017).

[5] Pfleging, W., "A review of laser electrode processing for development and manufacturing of lithium-ion batteries," Nanophotonics 7(3), 549–573 (2018).

[6] Habedank, J. B., Kriegler, J. and Zaeh, M. F., "Enhanced Fast Charging and Reduced Lithium-Plating by Laser-Structured Anodes for Lithium-Ion Batteries," J. Electrochem. Soc. 166(16), A3940-A3949 (2019).

[7] Dubey, R., Zwahlen, M.-D., Shynkarenko, Y., Yakunin, S., Fuerst, A., Kovalenko, M. V. and Kravchyk, K. V., "Laser Patterning of High-Mass-Loading Graphite Anodes for High-Performance Li-Ion Batteries," Batteries & Supercaps 4(3), 464–468 (2021).

[8] Park, D. and Lee, D., "Effect of Fluence and Multi-Pass on Groove Morphology and Process Efficiency of Laser Structuring for 3D Electrodes of Lithium-Ion Batteries," Materials (Basel, Switzerland) 14(5) (2021).

[9] Habedank, J. B., Endres, J., Schmitz, P., Zaeh, M. F. and Huber, H. P., "Femtosecond laser structuring of graphite anodes for improved lithium-ion batteries: Ablation characteristics and process design," Journal of Laser Applications 30(3), 32205 (2018).

[10] Nolte, S., Momma, C., Jacobs, H., Tünnermann, A., Chichkov, B. N., Wellegehausen, B. and Welling, H., "Ablation of metals by ultrashort laser pulses," Journal of the Optical Society of America B 14(10), 2716–2722 (1997).

[11] Kouli, M., Kandula, M. W. and Dilger, K., "Laser-material-interactions between ultrashort pulse lasers and electrodes for lithium-ion batteries during micro-structuring the electrode surface,", 46 (06.03.2021 - 12.03.2021).

[12] Pfleging, W. and Pröll, J., "A new approach for rapid electrolyte wetting in tape cast electrodes for lithium-ion batteries," J. Mater. Chem. A 2(36), 14918–14926 (2014).

[13] Neuenschwander, B., Jaeggi, B., Zimmermann, M. and Hennig, G., "Influence of particle shielding and heat accumulation effects onto the removal rate for laser micromachining with ultra-short pulses at high repetition rates,", 218–226 (2014).

[14] Jaeggi, B., Neuenschwander, B., Zimmermann, M., Penning, L., deLoor, R., Weingarten, K. and Oehler, A., “High-throughput and high-precision laser micromachining with ps-pulses in synchronized mode with a fast polygon line scanner,“ SPIE Proceedings, 89670Q (2014).
[15] Heimes, H. H., Kampker, A., Lienemann, C., Locke, M., Offermanns, C., Michaelis, S. and Rahimzei, E., Lithium-ion battery cell production process, PEM der RWTH Aachen University; DVMA, Aachen, Frankfurt am Main (2019).